Heliyon 8 (2022) e12276

Contents lists available at ScienceDirect

Heliyon

journal homepage: www.cell.com/heliyon

Research article

Neuroimaging biomarkers for detecting schizophrenia: A resting-state functional MRI-based radiomics analysis

Dafa Shi [a], Haoran Zhang [a], Guangsong Wang [a], Xiang Yao [a], Yanfei Li [a], Siyuan Wang [a], Ke Ren [a,b,*]

[a] Department of Radiology, Xiang'an Hospital of Xiamen University, School of Medicine, Xiamen University, Xiamen, 361002, China
[b] Xiamen Key Laboratory of Endocrine-Related Cancer Precision Medicine, Xiang'an Hospital of Xiamen University, School of Medicine, Xiamen University, Xiamen, 361002, China

ARTICLE INFO

Keywords:
Schizophrenia
Radiomics
Machine learning
Support vector machine
Functional connectivity
Voxel-mirrored homotopic connectivity
Degree centrality

ABSTRACT

Schizophrenia (SZ) is a common psychiatric disorder that is difficult to accurately diagnose in clinical practice. Quantifiable biomarkers are urgently required to explore the potential physiological mechanism of SZ and improve its diagnostic accuracy. Thus, this study aimed to identify biomarkers that classify SZ patients and healthy control subjects and investigate the potential neural mechanisms of SZ using degree centrality (DC)- and voxel-mirrored homotopic connectivity (VMHC)-based radiomics. Radiomics features were extracted from DC and VMHC metrics generated via resting-state functional magnetic resonance imaging, and significant features were selected and dimensionality was reduced using t-tests and least absolute shrinkage and selection operator. Subsequently, we built our model using a support vector machine classifier. We observed that our method obtained great classification performance (area under the curve, 0.808; accuracy, 74.02%), and it could be generalized to different brain atlases. The regions that we identified as discriminative features mainly included bilateral dorsal caudate and front-parietal, somatomotor, limbic, and default mode networks. Our findings showed that the radiomics-based machine learning method could facilitate us to understand the potential pathological mechanism of SZ more comprehensively and contribute to the accurate diagnosis of patients with SZ.

1. Introduction

Schizophrenia (SZ) is a complex psychiatric disorder. It is a major cause of disease burden worldwide (de Filippis et al., 2019; Li et al., 2020) with a global prevalence of approximately 1% (Bae et al., 2018; Cheng et al., 2015; Li et al., 2019a; Wang et al., 2020a). Psychological and behavioral indicators, rather than objective biological markers, are used in the diagnosis of SZ by the Diagnostic and Statistical Manual of Mental Disorders, 5th edition [DSM-5] (de Filippis et al., 2019; First et al., 2021) and International Classification of Diseases, 11th revision [ICD-11] (de Filippis et al., 2019; Reed et al., 2019). Diagnosing SZ is challenging in clinical practice and its underlying mechanism remains poorly understood (Bae et al., 2018; Plis et al., 2018; Wang et al., 2020a). Hence, quantifiable biomarkers would be evaluable for elucidating the neural mechanisms underlying SZ and to improve diagnostic accuracy (Bae et al., 2018; Chen et al., 2017a; de Filippis et al., 2019; Li et al., 2020; Wang et al., 2020a).

Magnetic resonance imaging (MRI) is a valuable, non-invasive method for studying of neuropsychiatric disorders. Two forms of MRI may be used: resting-state functional (rs-fMRI) (Rashid et al., 2020; Shi et al., 2021a,b; Zhao et al., 2020) and structural (sMRI) (Choi et al., 2022; Jiang et al., 2020; Wen et al., 2021; Zang et al., 2021). Previous studies (Jiang et al., 2020; Li et al., 2019a, 2020; Shi et al., 2021a; Wang et al., 2020a; Xiao et al., 2019) proposed that MRI measures could be used as potential biomarkers for SZ. Among them, functional connectivity (FC) is a commonly used metric and it can be static (Bohaterewicz et al., 2020; de Filippis et al., 2019; Jiang et al., 2020; Li et al., 2020; Orban et al., 2018; Plis et al., 2018) or dynamic (Luo et al., 2019; Sun et al., 2019; Weber et al., 2020; Zhang et al., 2021). However, conventional FC evaluates connectivity patterns between predefined brain regions or distinct brain network components via independent component analysis (ICA). Degree centrality (DC) and voxel-mirrored homotopic connectivity (VMHC) are new rs-fMRI indicators used to evaluate FCs across the whole brain at a voxel level (Jiang et al., 2019; Li et al., 2019b; Zhang et al., 2019). More work is needed in order to determine the utility of DC

* Corresponding author.
E-mail address: renke815@sina.com (K. Ren).

https://doi.org/10.1016/j.heliyon.2022.e12276
Received 18 February 2022; Received in revised form 19 May 2022; Accepted 2 December 2022
2405-8440/© 2022 Published by Elsevier Ltd. This is an open access article under the CC BY-NC-ND license (http://creativecommons.org/licenses/by-nc-nd/4.0/).

and VMHC for SZ (de Filippis et al., 2019; Shan et al., 2021; Shi et al., 2021a).

Radiomics, an emerging method of medical image analysis, has rapidly developed to identify brain signatures for neuropsychological diseases aiding in diagnosis, prediction, and identification of physiological mechanisms (Feng et al., 2018; Shi et al., 2021b, 2022; Sun et al., 2018; Zhao et al., 2020). In radiomics analysis, medical images can be transformed into high-throughput, quantitative, and mineable features, including some invisible to the human visual system, by a series of data characterization algorithms (Gillies et al., 2016; Lambin et al., 2012). Machine learning techniques are also used to perform data mining on extracted features. Currently, there is growing use of rs-fMRI-based radiomics analysis for exploring neuroimaging biomarkers of neuropsychiatric disorders, including AD (Feng et al., 2018; Zhao et al., 2020), attention deficit hyperactivity disorder (Sun et al., 2018), hippocampal sclerosis (Mo et al., 2019), and PD (Shi et al., 2021b, 2022). To our knowledge, no studies have assessed SZ diagnosis with DC- and VMHC-based radiomics.

Therefore, this study aimed to identify biomarkers that classify SZ patients and healthy control subjects (HCs) and investigate the potential neural mechanisms of SZ with DC- and VMHC-based radiomics.

2. Materials and methods

2.1. Study subjects

We retrieved data for 72 SZ patients and 74 HCs matched for age and sex from the Center for Biomedical Research Excellence (COBRE), an open-source data repository hosted on the Neuroimaging Informatics Tools & Resources Collaboratory. Details of the participants are available in previous studies (Shi et al., 2021a; Xue et al., 2019) and online (http://fcon_1000.projects.nitrc.org/indi/retro/cobre.html). We excluded participants with incomplete imaging information (SZ, n = 1) and substantial head motion (>2° or 2 mm, SZ, n = 15; HC, n = 8). A total of 122 participants (66 HCs and 56 patients with SZ) were included. Demographic information is listed in Table 1. The COBRE investigators received ethical approval and participants provided written informed consent.

2.2. Data acquisition

Participants underwent sMRI and rs-fMRI scans in a 3-T Trio Tim Scanner (Siemens). Protocols have been reported previously (Li et al., 2019a; Shi et al., 2021a; Xue et al., 2019) and they are available online (http://fcon_1000.projects.nitrc.org/indi/retro/cobre.html). Detailed parameters for MRI data acquisition are provided in **Supplemental Methods**.

2.3. Data preprocessing and DC and VMHC calculation

The data preprocessing and DC and VMHC calculation procedures were performed as described elsewhere (Shi et al., 2021a). Data preprocessing was completed using Data Processing & Assistant for Brain Imaging (DPABI) (Yan et al., 2016) and Statistical Parametric Mapping (SPM12). Preprocessing consisted of volume removal (first 10); correction of slice timing; realignment correction; segmentation using new segment; image registration using Diffeomorphic Anatomical Registration Through Exponentiated Lie Algebra (DARTEL); spatial normalization by DARTEL (resampling: $3 \times 3 \times 3$ mm^3); removal of nuisance covariates, including white matter, cerebrospinal fluid signal, linear trend, and Friston 24 head motion parameters; bandpass filter (0.01–0.10 Hz). The global signal was not regressed as it may contain important information about the neuronal activity in SZ (Shi et al., 2021a; Umeh et al., 2020; Yang et al., 2017; Yang et al., 2014). For VMHC, we performed two additional preprocessing procedures: the preprocessed images were registered to a symmetric template to ensure correspondence between symmetric voxels of the two hemispheres and smoothed [Gaussian kernel, full width at half-maximum (FWHM) = 4 mm].

Default DPABI software settings were used to calculate DC and VMHC maps. Pearson's correlation was used to correlate time courses of voxel pairs, and the correlation coefficient threshold ($r > 0.25$) was set to construct an undirected adjacency matrix. Subsequently, the DC maps were determined as the weighted sum of the positive connections of the voxels and smoothed (Gaussian kernel, FWHM = 4 mm). Pearson's correlations of the time courses between each voxel and the contralateral hemisphere's mirror voxel were calculated to obtain VMHC maps. Fisher's z-transformations were performed on the resulting DC and VMHC maps.

2.4. Feature extraction

In-house scripts were used to extract quantitative radiomics features. Two hundred forty-six volumes of interest (VOIs) were segmented from the individual DC and VMHC maps using Brainnetome 246 atlas (Fan et al., 2016) (**Supplementary Methods**). We extracted 48 radiomics features for each VOI, including 15 intensity-based histogram and 33 texture features, which measure the intensity of gray levels and the spatial dissimilarity of the intensity levels for all voxels in VOI, respectively. Additional details are described elsewhere (Aerts et al., 2014; Feng et al., 2018; Shi et al., 2022; Zhao et al., 2020) and in **Supplementary Methods**. Finally, a total of 23,616 features [$(15 + 33) \times 246 \times 2 = 23616$] were extracted from each participant. The full process for feature extraction is shown in Figure 1A and B.

2.5. Feature selection and construction and evaluation of model

Features were selected and dimensionality was reduced using t-tests and least absolute shrinkage and selection operator (LASSO). Nested ten-fold cross-validation was employed to evaluate model performance and tune the hyperparameter (optimal λ of LASSO). The outer loop served to assess classifier performance while the optimal λ was selected by the inner loop. The classification model was then built using a support vector machine (SVM) classifier. The complete procedure is shown in Figure 1C and D and Supplementary Figure S1, and it was reported previously (Shi et al., 2022).

Features were standardized to z-scores to reduce the effect of the units introduced by the features and improve model performance. Since the dimension of the feature was significantly higher than the sample size and many of the features may be redundant, irrelevant, or uninformative, we performed dimensionality reduction to speed up the computation and improve the reliability of our model. First, features distinguishing SZ patients from HCs were selected using two-sample two-tailed t-tests. Then, LASSO was used to identify the most important features. For LASSO, the regulation parameter λ tuned the model sparsity. A grid search (0.01–0.4, 0.01 interval) method was performed within ten-fold cross-validation to tune the hyperparameter (Chen et al., 2016, 2017b; Zhao et al., 2018a), which we defined as having the highest classification accuracy (Supplementary Figure S1).

The SVM classifier (linear kernel function and C = 1) was adopted to estimate the state (patient with SZ or HC) of each participant, and we

Table 1. Demographic characteristics of schizophrenia patients and healthy controls.

	SZs	HCs	Statistic	*P* value
Sample size	56	66		
Age (years)	38.32 ± 14.04	36.03 ± 11.96	0.97[a]	0.33
Gender			1.66[b]	0.20
Male	44	45		
Female	12	21		

[a] The t value was obtained by t-test.
[b] The chi-squared value was calculated by chi-squared test.

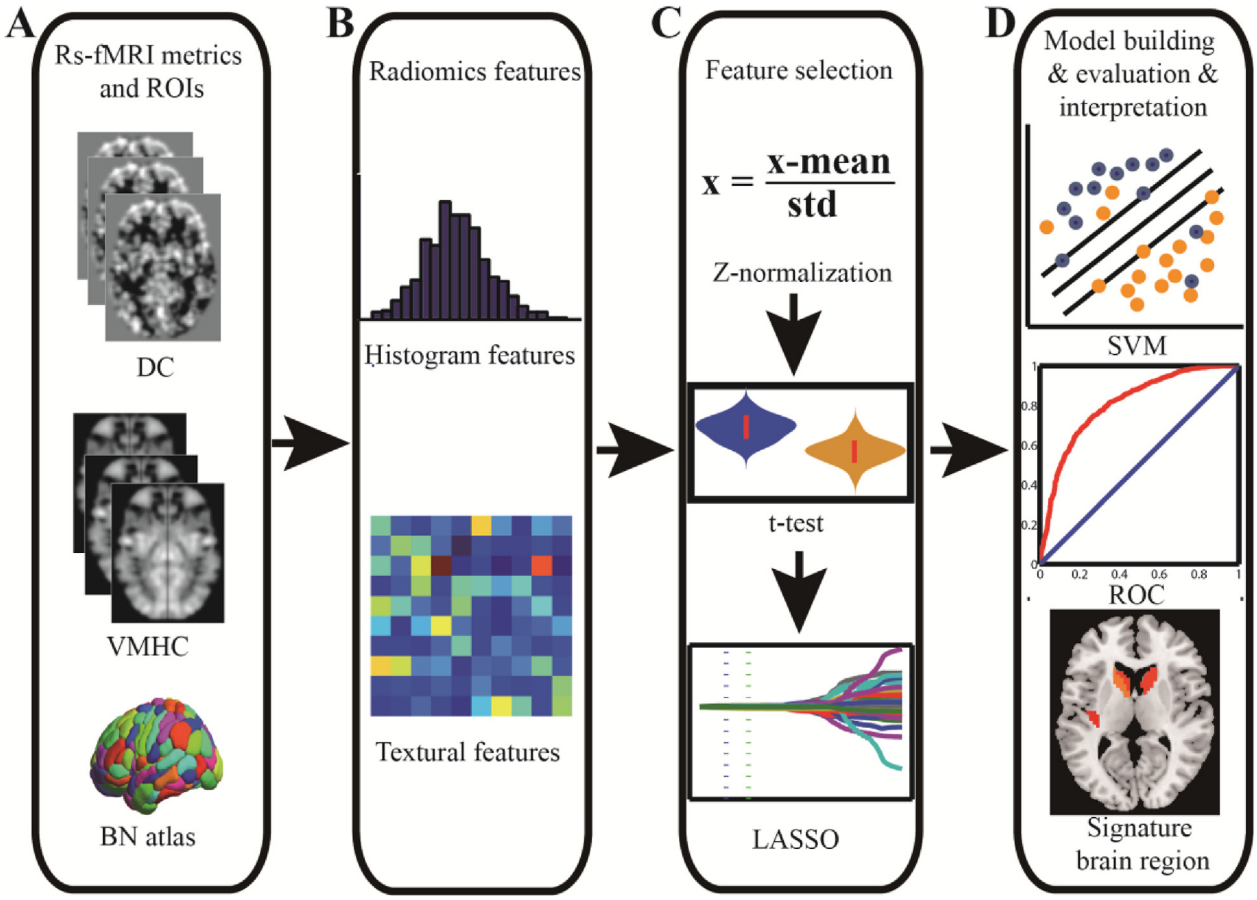

Figure 1. Schematic detailing of the study procedure. (A) Functional MRI measures (DC and VMHC) and Brainnetome 246 atlas. (B) Intensity-based histogram and textural features were extracted from DC and VMHC images. (C) Two-sample t-tests and LASSO were performed for feature selection. (D) An SVM model was built and ROC curve analysis was applied to evaluate model performance, and we identified discriminative features. Abbreviations: DC, degree centrality; VMHC, voxel-mirrored homotopic connectivity; BN, Brainnetome; LASSO, least absolute shrinkage and selection operator; SVM, support vector machine; ROC, receiver operating characteristic.

employed ten-fold cross-validation to assess classifier performance (repeated 20 times). We assessed mean accuracy, balance accuracy, area under the curve (AUC), F1 score, sensitivity, specificity, and precision across all iterations (10 folds × 20 times) using receiver operating characteristic (ROC) curve analysis to evaluate the model's performance. Performance evaluation is described elsewhere (Shi et al., 2022; Zheng et al., 2019; Zhou et al., 2020b) and in the **Supplementary Methods**.

Classification performance (AUC and accuracy) significance was evaluated by permutation test (Geng et al., 2018; Hu et al., 2019; Shi et al., 2021a; Zhou et al., 2020a). Specifically, class labels (patients with SZ or HC) were permuted 1,000 times, and then the classification procedure was applied to get the permutated AUCs and accuracies. *P*-values were calculated using the following formula:

$$P = (1 + N_{\text{greater performance}})/(1 + 1000)$$

where $N_{\text{greater performance}}$ is the permutation times that achieve higher performance (AUC and accuracy) than the actual value.

2.6. Identification of discriminative features

Model performance was determined by ten-fold cross-validation. The sample subset was slightly different for each iteration, and thus so were the features selected for each iteration. We sorted the occurrence frequencies of the features that were selected across each cross-validation run (200 iterations) and selected the top 10 features of two measures (DC and VMHC) as the discriminative features (Cui et al., 2016; Shi et al., 2022; Yang et al., 2019; Zhao et al., 2020; Zhou et al., 2020a). As the SVM classification model was applied with a linear kernel, the weights of features in the model were obtained and the mean weights across all iterations were calculated. A positive weight indicates that there was a higher measurement of the discriminative feature of SZ patients than HCs relative to the hyper-plane, whereas a negative weight indicates that the measurement of HCs was higher than that of SZ patients relative to the hyper-plane (Ecker et al., 2010; Yin et al., 2021). A higher weight's absolute value reflects a greater contribution to the classification.

2.7. Validating the performance

To assess the generalizability of our method to other brain atlases, Shen 268 (Shen et al., 2013) and automated anatomical labeling (AAL) 90 (Tzourio-Mazoyer et al., 2002) atlases were used. To be consistent with AAL 90 and Brainnetome 246 atlases, VOIs of the cerebellum and brainstem were excluded from the Shen 268 atlas in our study. We performed the same procedure mentioned above and assessed model performance.

3. Results

3.1. Demographic information

In total, 122 participants (56 SZ patients and 66 HCs) were included. Demographic data are shown in Table 1. Age and sex did not differ between groups.

Table 2. Classifier performances for different brain atlases.

	Accuracy	AUC	Sensitivity	Specificity	Precision	F1 score	balance accuracy	*P* value (AUC)	*P* value (accuracy)
BN 246	74.02%	0.808	69.11%	78.18%	72.88%	70.94%	73.64%	0.001	0.001
AAL 90	66.43%	0.722	62.77%	69.55%	63.62%	63.19%	66.16%	0.001	0.002
Shen 268	72.21%	0.785	69.02%	74.92%	70.02%	69.51%	71.97%	0.001	0.001

Abbreviations: BN, Brainnetome atlas; AAL, automated anatomical labeling atlas; AUC, area under the curve.

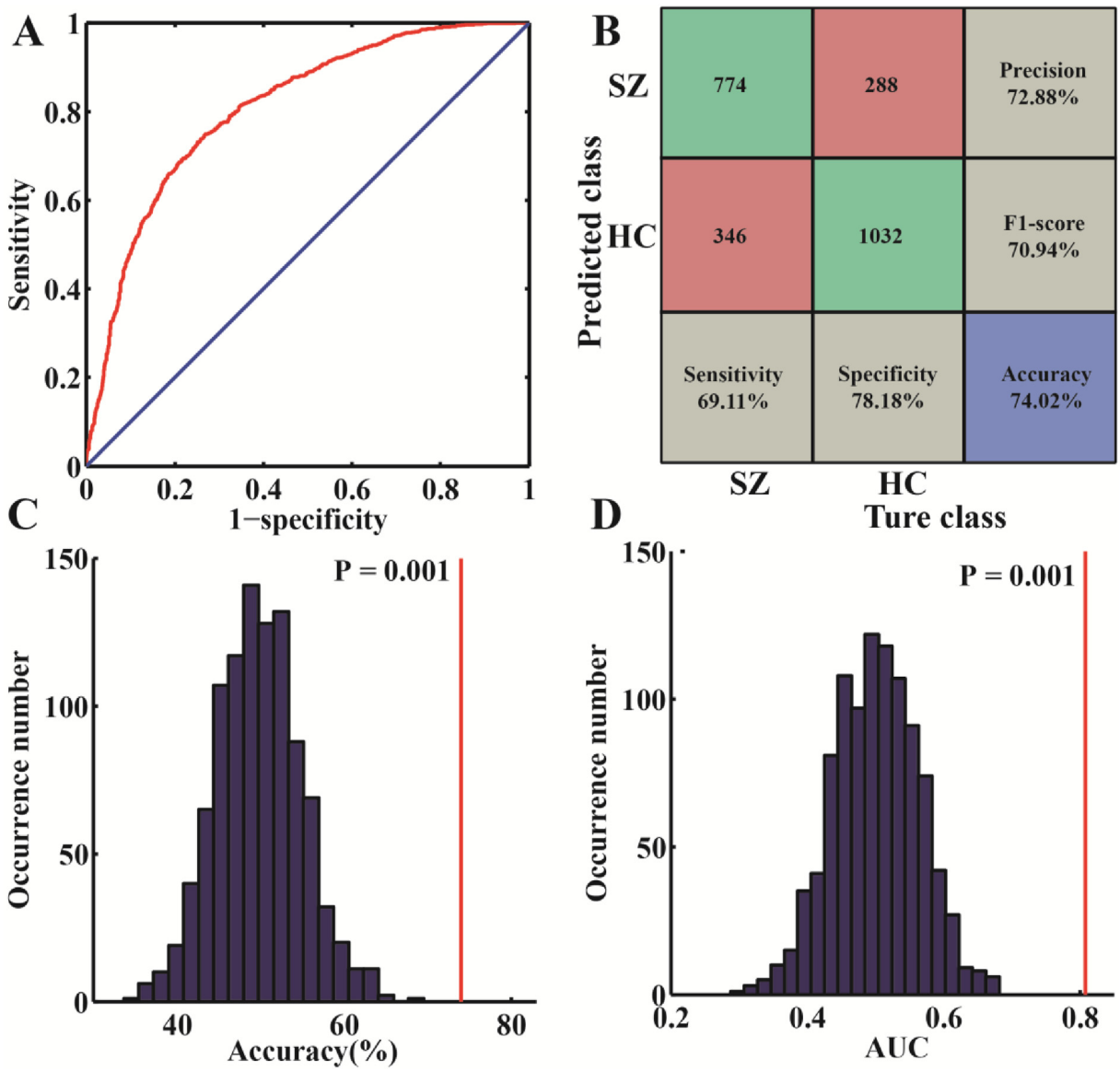

Figure 2. Classification performances with Brainnetome 246 atlas and ten-fold cross-validation (repeated 20 times). The ROC curve (A) and confusion matrix (B) for the classification of patients with SZ and HCs. The distributions of the permutated accuracies (C) and AUCs (D). The red lines represent the real accuracy (C) and AUC (D). Abbreviations: SZ, schizophrenia; HC, healthy controls; AUC, area under the curve.

3.2. Classification performance

The optimal λ of LASSO was tuned using the grid search method based on classification accuracy with nested ten-fold cross-validation. AUC and accuracy were 0.808 and 74.02%, respectively, and when compared with chance using a permutation test, both were significantly higher than chance (both $P < 0.05$). Mean AUC, accuracy, balance accuracy, F1 score, sensitivity, specificity, precision, and *P*-values of AUC and accuracy are reported in Table 2 and Figure 2A, B, C, D.

3.3. Discriminative features

To identify the features that made the most substantial contribution to the classification model, we reported discriminative features, which were the top 10 features selected for all iterations (10 folds × 20 times) and calculated the mean weights of the features (Table 3, Figures 3 and 4). The discriminative brain regions we identified included the bilateral basal ganglia (BG), parahippocampal gyrus (PhG), left medioventral occipital cortex (MVOcC), middle frontal gyrus (MFG), precentral gyrus

Table 3. Discriminative features for schizophrenia classification.

Measures	Lobe	Gyrus regions	Anatomical and modified Cyto-architectonic descriptions	Feature	Weight	Yeo 7 Network
DC	Occipital Lobe	MVOcC _L_5_1	caudal lingual gyrus	median	−0.781	Visual
	Subcortical Nuclei	BG_R_6_5	dorsal caudate	Cluster Shade	−0.281	-
	Temporal Lobe	ITG_R_7_6	caudolateral of area 20	Homogeneity1	−0.338	Frontparietal
	Subcortical Nuclei	BG_L_6_1	ventral caudate	Correlation	−0.289	-
	Frontal Lobe	PrG_L_6_3	upper limb region	Sum Entropy	−0.314	Somatomotor
	Subcortical Nuclei	BG_L_6_5	dorsal caudate	LRLRE	−0.436	-
	Insular Lobe	INS_L_6_1	hypergranular insula	Cluster Prominence	−0.187	Somatomotor
	Temporal Lobe	ITG_R_7_6	caudolateral of area 20	Homogeneity2	−0.470	Frontparietal
	Temporal Lobe	FuG_L_3_1	rostroventral area 20	Autocorrelation	0.320	Limbic
	Temporal Lobe	PhG_L_6_1	rostral area 35	Correlation	0.238	Limbic
VMHC	Subcortical Nuclei	BG_R_6_5	dorsal caudate	skewness	−0.625	-
	Subcortical Nuclei	Tha_R_8_2	pre-motor thalamus	Contrast	−0.340	-
	Parietal Lobe	PoG_R_4_2	tongue and larynx region	Sum Entropy	−0.235	Somatomotor
	Subcortical Nuclei	Tha_R_8_2	pre-motor thalamus	IDMN	0.568	-
	Temporal Lobe	MTG_L_4_2	rostral area 21	LRE	−0.186	Default
	Subcortical Nuclei	Amyg_L_2_2	lateral amygdala	Energy	−0.107	-
	Subcortical Nuclei	Hipp_R_2_2	caudal hippocampus	Variance	0.097	-
	Temporal Lobe	PhG_R_6_4	entorhinal cortex	LRLGLE	−0.148	Limbic
	Temporal Lobe	MTG_L_4_1	caudal area 21	range	0.194	Default
	Frontal Lobe	MFG_L_7_5	ventrolateral area 8	maximum	0.237	Default

Abbreviations: DC: degree centrality; VMHC: voxel-mirrored homotopic connectivity; MVOcC, medioventral occipital cortex; BG, basal ganglia; ITG, inferior temporal gyrus; PrG, precentral gyrus; INS, insular gyrus; ITG, inferior temporal gyrus; FuG, fusiform gyrus; PhG, parahippocampal gyrus; Tha, thalamus; PoG, postcentral gyrus; MTG, middle temporal gyrus; Amyg, amygdala; Hipp, hippocampus; MFG, middle frontal gyrus; LGLRE, low gray level run emphasis; IDMN, inverse difference moment normalized; LRE, long run emphasis; LRLGLE, long run low gray level emphasis; L, left; R, right.

(PrG), insular gyrus (INS), fusiform gyrus (FuG), middle temporal gyrus (MTG), amygdala, right postcentral gyrus (PoG), inferior temporal gyrus (ITG), thalamus, and hippocampus. They were mainly located in subcortical nuclei (bilateral dorsal caudate), front-parietal, somatomotor, limbic, and default mode networks.

3.4. Validation analysis

When we performed our analysis procedure using AAL 90 and Shen 268 atlases, we found that our method also achieved great classification performances. Brainnetome 246 atlas had the best performance and AAL 90 atlas had the worst performance (Table 2 and Supplementary Figures S2 and S3).

4. Discussion

In this study, we employed an SVM classifier to identify SZ patients and HCs using DC- and VMHC-based radiomics analysis. We determined the method we proposed had strong classification performance (Brainnetome 246 atlas: AUC = 0.808, accuracy = 74.02%), and it was robust and could be generalized to different atlases (AAL 90 atlas: AUC = 0.722, accuracy = 66.43%; Shen 268 atlas: AUC = 0.785, accuracy = 72.21%). Our study also demonstrated that our procedure was able to identify quantitative DC- and VMHC-based biomarkers which could distinguish patients with SZ from HCs and explain the neural mechanism underlying SZ. This study is the first that we are aware of to discover rs-fMRI-based biomarkers of SZ by DC- and VMHC-based radiomics analysis.

The rs-fMRI values in neuropsychiatric disorders have been confirmed (Li et al., 2019a; Qiu et al., 2020; Zhao et al., 2020; Zhou et al., 2020a), including SZ (Bohaterewicz et al., 2020; Li et al., 2019a, 2020; Xiao et al., 2019). Among them, FC is a commonly used indicator (Bohaterewicz et al., 2020; Li et al., 2019a; Lin et al., 2020). However, conventional FC evaluates connectivity patterns between predefined specific brain regions or distinct brain network components by the ICA method. Both methods are useful but do not reveal the entire connectivity pattern of the brain elements at a voxel level (Jiang et al., 2019). Moreover, voxel-wise FC is computationally expensive and it is difficult to interpret the results. DC and VMHC are new rs-fMRI indicators used to evaluate FCs across the whole brain at a voxel level. DC, a data-derived measurement method, measures the FC strengths across the entire brain at a voxel level and may proxy the global brain activity synchronizations or FC density (Buckner et al., 2009; Li et al., 2019b). VMHC reflects the homotopic FC between the two hemispheres by determining the correlation coefficient between voxel and the contralateral hemisphere's mirror voxel (Lu et al., 2021; Shan et al., 2021). The two measures do not rely on prior information about the target brain regions. Therefore, DC and VMHC may be more appropriate than conventional FC in studying neuropsychiatric disorders whose pathological mechanisms were unclear (Jiang et al., 2019). We found that DC and VMHC are physiologically meaningful and beneficial in understanding the underlying mechanism of SZ, DC- and VMHC-based features can distinguish SZ patients from HCs, in agreement with other studies (de Filippis et al., 2019; Liu et al., 2018; Shan et al., 2021; Shi et al., 2021a; Tang et al., 2019; Zang et al., 2021).

Radiomics can be used to generate high-throughput quantitative features from medical imaging. Machine learning algorithms are also employed in data mining (Gillies et al., 2016; Lambin et al., 2012). Other studies have applied radiomics to identify neuroimaging biomarkers of neuropsychiatric diseases (Feng et al., 2018; Mo et al., 2019; Sun et al., 2018; Wang et al., 2020b; Zhao et al., 2020). SVM is a widely-adopted machine learning algorithm, especially in studies with relatively limited sample sizes, such as neuroimaging studies (Hong et al., 2017; Shu et al., 2021; Talai et al., 2021; Tian et al., 2020; Zhang et al., 2021). It is extensively applied in the classification of neuropsychiatric disorders (Feng et al., 2018; Mo et al., 2019; Wang et al., 2020b; Zhao et al., 2020). SVM combines several favorable attributes to minimize overfitting and provide good generalization capability even with small sample sizes (Hong et al., 2017; Mo et al., 2019). We used DC and VMHC maps to extract intensity-based histogram and texture features and we classified SZ patients and HCs using an SVM classifier. Our method had great

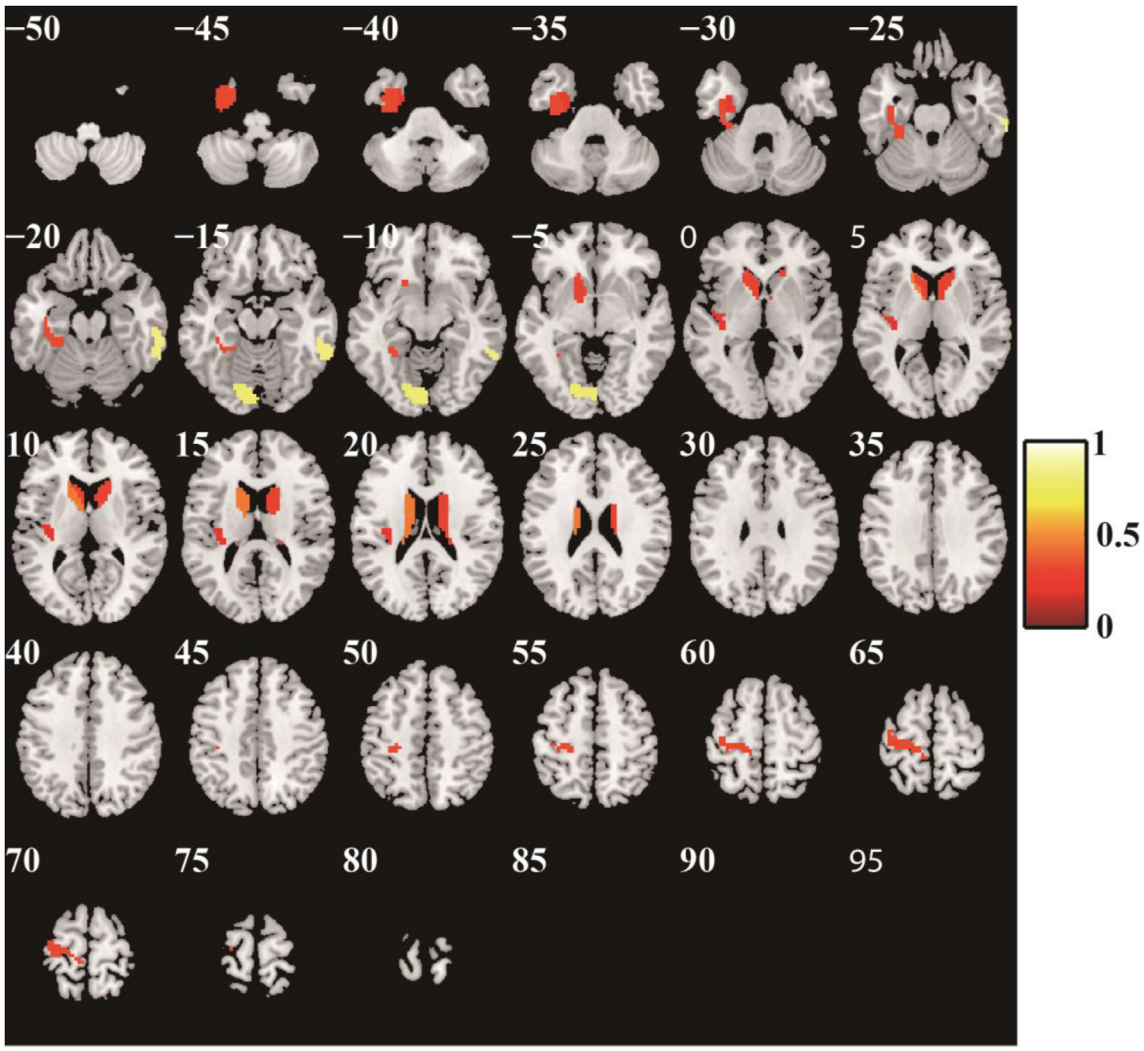

Figure 3. Discriminative brain regions for degree centrality. The discriminative regions included bilateral basal ganglia, left medioventral occipital cortex, precentral gyrus, insular gyrus, fusiform gyrus and right inferior temporal gyrus. The colored bar represents the weight's absolute value of the brain regions.

classification performance with 74.02% of accuracy and 0.808 of AUC, and we identified discriminative features that distinguish SZ patients and HCs, in agreement with the other studies.

We determined that our method also has strong classification performances with AAL 90 and Shen 268 atlases (AAL 90 atlas: accuracy = 66.43%, AUC = 0.722; Shen 268 atlas: accuracy = 72.21%, AUC = 0.785), which demonstrates that our method is robust and generalizable (Shi et al., 2021a; Wang et al., 2020b). In addition, AAL 90 atlas had the worst performance among the three atlases, while Brainnetome 246 atlas had the best performance, consistent with previous studies. Other approaches may be better for detecting disease-related differences, including functionally defined and high spatial resolution segmentation. In addition, the anatomical and functional boundaries may not coincide (Chen et al., 2018; Rosenberg et al., 2016). These could explain why the classification performances of Brainnetome 246 and Shen 268 atlases are more accurate (Chen et al., 2018; Shi et al., 2021a).

Previous studies have mostly used group-level comparison analysis (Lu et al., 2021; Xue et al., 2019; Yan et al., 2020; Zhao et al., 2018b) or machine learning (Bohaterewicz et al., 2020; Li et al., 2019a, 2020) to evaluate the spontaneous neural activity abnormalities of SZ patients. This study was the first that we are aware of to apply a radiomics-based machine learning method with DC and VMHC metrics to detect SZ potential biomarkers and explore the potential biological mechanism of SZ.

In this work, we determined that the discriminative brain regions include the bilateral BG, PhG, left MVOcC, PrG, INS, FuG, MTG, amygdala, MFG, right ITG, thalamus, PoG, and hippocampus. The MVOcC is an important component of the visual network. Many studies have reported abnormalities in the visual network regions (including MVOcC) of SZ patients (de Filippis et al., 2019; Gong et al., 2020; Shi et al., 2021a; Tohid et al., 2015; Xue et al., 2019; Zhao et al., 2018b). Our study identified DC abnormalities in the left MVOcC in SZ; the result is in agreement with the other studies. In this study, many brain regions showing abnormalities in VMHC belong to the default mode network (DMN), such as MTG and MFG. Recently, a growing body of literature has assessed the crucial roles of disrupted DMN connectivity and abnormal brain activity in the neural mechanisms underlying SZ and DMN disturbances are closely associated with SZ psychopathology and cognitive impairment (Gong et al., 2020; Hu et al., 2017; Mingoia et al., 2012; Schneider et al., 2011; Shan et al., 2021; Wen et al., 2021; Yan et al., 2020; Zhao et al., 2018b, 2019). The amygdala, hippocampus, FuG, and PhG are important parts of the limbic system, which regulates instinctive, cognitive, and emotional behavior. Many studies have indicated that abnormal activities of the limbic system were the basis of SZ symptoms (Ma et al., 2019; Tang et al., 2019; Wen et al., 2021). Prior studies also reported abnormal brain neural activity in somatomotor network (including PrG, INS, and PoG) (de Filippis et al., 2019; Gong et al., 2020;

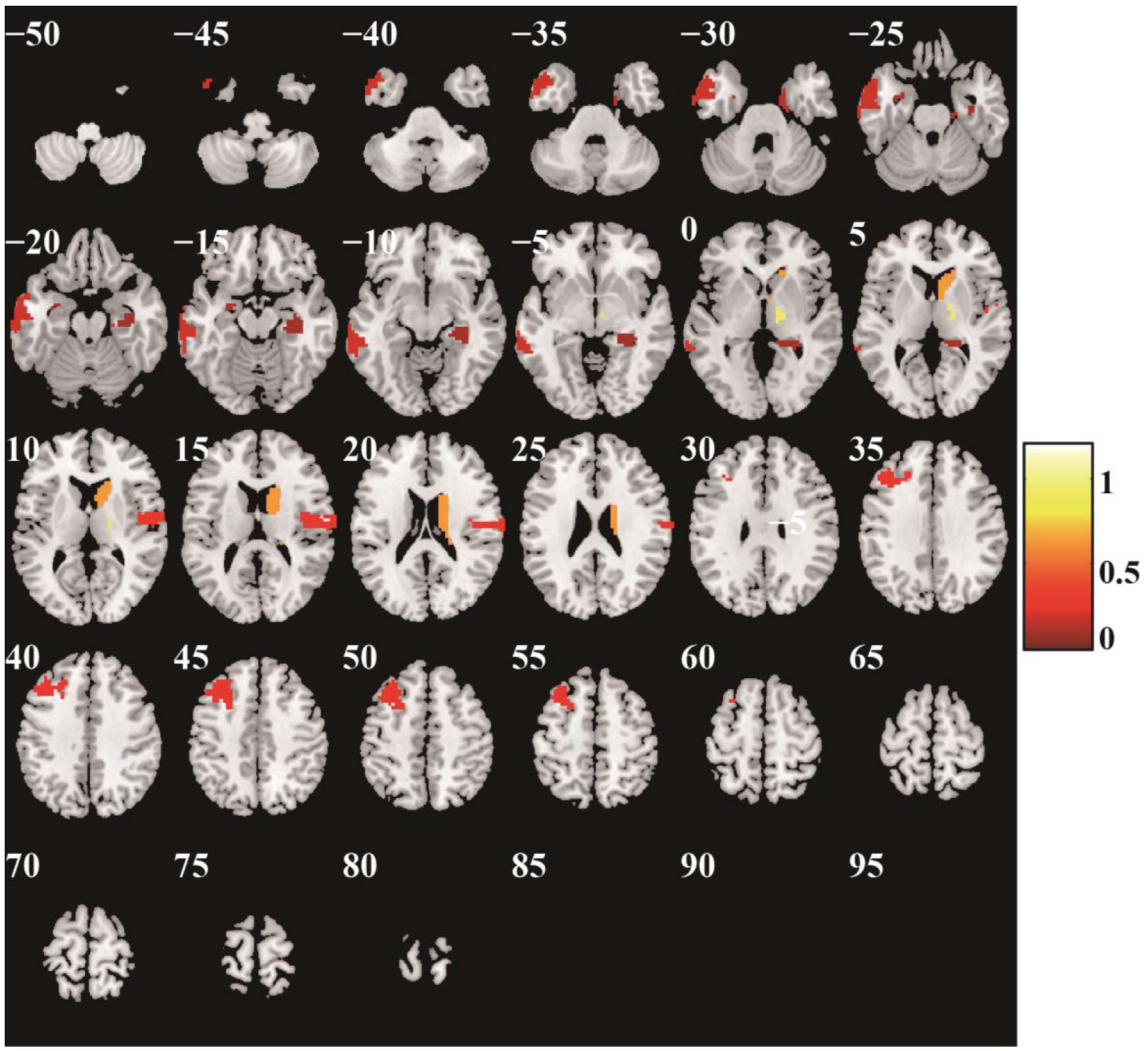

Figure 4. Discriminative brain regions for voxel-mirrored homotopic connectivity. The discriminative regions included the left middle temporal gyrus, amygdala, middle frontal gyrus, right basal ganglia, thalamus, postcentral gyrus and hippocampus and parahippocampal gyrus. The colored bar represents the weight's absolute value of the brain regions.

Liu et al., 2018; Wu et al., 2018). The PrG is involved in social cognition, which includes the perception of facial expressions, moods, and personal desire and it plays a role in SZ pathology (Zhao et al., 2019). A recent study (Gong et al., 2020) suggested that reduced intrinsic activity in the PoG might serve as a differentiating feature of chronic SZ. Many studies have indicated that negative emotions and behaviors are linked to functional and structural abnormalities in the temporal lobe (Dai et al., 2019; DeWitt et al., 2018; Fang et al., 2021), and in SZ patients, ITG was associated with depressive symptom severity and the score of the Positive and Negative Syndrome Scale (PANSS) (Fang et al., 2021; Gong et al., 2020). Our results agree with these studies.

We also found abnormalities in the subcortical nuclei, including BG (bilateral dorsal caudate and left amygdala) and right thalamus (premotor thalamus). The caudate is a part of the striatum with key dopaminergic function, and the striatum plays a role in the SZ pathology (Li et al., 2020; Simpson et al., 2010; Zhao et al., 2018b), and neuroimaging methods also detected abnormal neural activity in the caudate (Cui et al., 2018; Li et al., 2020; Tang et al., 2019; Wen et al., 2021; Xue et al., 2019; Zhao et al., 2018b). Wulff et al. (2020) detected reduced blood-oxygen-level-dependent (BOLD) signal in the caudate nucleus after treatment in patients with SZ, and improvements in the BOLD signal were correlated with the treatment response on positive symptoms and the occupancy of D2 receptors. In our study, we found that the feature of the caudate was an important neuroimaging biomarker. The hippocampus is recognized as a critical brain region in the pathophysiology of SZ, as it is essential in declarative memory, mood, and stress (Choi et al., 2022; Haijma et al., 2013). Choi et al. (2022) indicated that changes in hippocampal subregional volumes could be used as biomarkers to recognize the impacts of genetic risk for SZ. Zhao et al. (2019) found that regional homogeneity in the right thalamus was correlated with depressed and positive factors of PANSS score.

This study has limitations. First, although there is a larger sample size than other studies evaluating SZ using machine learning (de Filippis et al., 2019; Shan et al., 2021; Wang et al., 2020a), the sample size is still small and increasing the sample and centers will make the findings more generalizable. Second, prior studies have identified the presence of abnormal cerebellum activation in SZ patients (de Filippis et al., 2019; Shan et al., 2021; Xie et al., 2021). Thus, cerebellar DC and VMHC abnormalities may be potential biomarkers of SZ. In this study, we applied the Brainnetome 246 atlas, which excludes the cerebellum for VOI segmentation, to extract the radiomics features. The Brainnetome 246 atlas is a functionally defined and high spatial resolution parcellation, and it has a well-defined anatomical and functional localization. We found that it could achieve greater classification performance. Third, other machine learning techniques, such as deep learning (Oh et al., 2019; Qiu et al., 2020), especially deep neural networks (DNN) (Rahaman et al., 2021;

Zeng et al., 2018; Zheng et al., 2021), may improve the performance of patients with SZ classification. Studies (Rahaman et al., 2021; Zeng et al., 2018; Zheng et al., 2021) have confirmed that DNNs can perfectly classify SZ, explain the underlying mechanisms and provide the most salient features for classification. In the future, we will explore deep learning approaches to improve classification performance and to identify more sensitive and stable biomarkers. Fourth, incorporating multimodal data can improve the model's performance (Talai et al., 2021). Jiang et al. (2020) confirmed the disrupted functional organization of white and gray matter in SZ. For future work, we will integrate functional and structural MRI data to further explore abnormalities in the structural and functional organization of SZ. Fifth, our study applied an atlas to segment VOIs to identify potential biomarkers for SZ. ICA-based parcellation has been applied to segment VOIs (Damaraju et al., 2014; Rahaman et al., 2022), using decomposition and k-means clustering to extract potential biomarkers/discriminating brain regions. In the future, we will try this method and compare it with our proposed method.

5. Conclusion

In conclusion, we found that the radiomics-based machine learning method we proposed based on DC and VMHC metrics could classify patients with SZ and HCs with great performance, and it had good robustness and generalizability. Moreover, rs-fMRI-based radiomics is an effective method to identify SZ neuroimaging biomarkers, which may be the pathological mechanism underlying SZ. These findings help elucidate the potential neural mechanism of SZ and may contribute to the accurate diagnosis of SZ patients.

Declarations

Author contribution statement

Dafa Shi: Conceived and designed the experiments; Performed the experiments; Analyzed and interpreted the data; Wrote the paper.

Haoran Zhang, Guangsong Wang: Performed the experiments; Analyzed and interpreted the data; Wrote the paper.

Xiang Yao, Yanfei Li, Siyuan Wang: Performed the experiments.

Ke Ren: Conceived and designed the experiments; Analyzed and interpreted the data.

Funding statement

Ke Ren was supported by Scientific Research Foundation for Advanced Talents, Xiang'an Hospital of Xiamen University [PM201809170011].

Data availability statement

Data included in article/supp. material/referenced in article.

Declaration of interest's statement

The authors declare no conflict of interest.

Additional information

Supplementary content related to this article has been published online at https://doi.org/10.1016/j.heliyon.2022.e12276.

References

Aerts, H.J., Velazquez, E.R., Leijenaar, R.T., Parmar, C., Grossmann, P., Carvalho, S., Lambin, P., 2014. Decoding tumour phenotype by noninvasive imaging using a quantitative radiomics approach. Nat. Commun. 5 (1), 4006.

Bae, Y., Kumarasamy, K., Ali, I.M., Korfiatis, P., Akkus, Z., Erickson, B.J., 2018. Differences between schizophrenic and normal subjects using network properties from fMRI. J. Digit. Imag. 31 (2), 252–261.

Bohaterewicz, B., Sobczak, A.M., Podolak, I., Wojcik, B., Metel, D., Chrobak, A.A., Marek, T., 2020. Machine learning-based identification of suicidal risk in patients with schizophrenia using multi-level resting-state fMRI features. Front. Neurosci. 14, 605697.

Buckner, R.L., Sepulcre, J., Talukdar, T., Krienen, F.M., Liu, H., Hedden, T., Johnson, K.A., 2009. Cortical hubs revealed by intrinsic functional connectivity: mapping, assessment of stability, and relation to Alzheimer's disease. J. Neurosci. 29 (6), 1860–1873.

Chen, X., Liao, X., Dai, Z., Lin, Q., Wang, Z., Li, K., He, Y., 2018. Topological analyses of functional connectomics: a crucial role of global signal removal, brain parcellation, and null models. Hum. Brain Mapp. 39 (11), 4545–4564.

Chen, X., Liu, C., He, H., Chang, X., Jiang, Y., Li, Y., Yao, D., 2017a. Transdiagnostic differences in the resting-state functional connectivity of the prefrontal cortex in depression and schizophrenia. J. Affect. Disord. 217, 118–124.

Chen, X., Zhang, H., Gao, Y., Wee, C.Y., Li, G., Shen, D., Alzheimer's Disease Neuroimaging, I., 2016. High-order resting-state functional connectivity network for MCI classification. Hum. Brain Mapp. 37 (9), 3282–3296.

Chen, X., Zhang, H., Zhang, L., Shen, C., Lee, S.W., Shen, D., 2017b. Extraction of dynamic functional connectivity from brain grey matter and white matter for MCI classification. Hum. Brain Mapp. 38 (10), 5019–5034.

Cheng, H., Newman, S., Goni, J., Kent, J.S., Howell, J., Bolbecker, A., Hetrick, W.P., 2015. Nodal centrality of functional network in the differentiation of schizophrenia. Schizophr. Res. 168 (1-2), 345–352.

Choi, S., Kim, M., Park, H., Kim, T., Moon, S.Y., Lho, S.K., Kwon, J.S., 2022. Volume deficits in hippocampal subfields in unaffected relatives of schizophrenia patients with high genetic loading but without any psychiatric symptoms. Schizophr. Res. 240, 125–131.

Cui, L.B., Liu, L., Wang, H.N., Wang, L.X., Guo, F., Xi, Y.B., Yin, H., 2018. Disease definition for schizophrenia by functional connectivity using radiomics strategy. Schizophr. Bull. 44 (5), 1053–1059.

Cui, Z., Xia, Z., Su, M., Shu, H., Gong, G., 2016. Disrupted white matter connectivity underlying developmental dyslexia: a machine learning approach. Hum. Brain Mapp. 37 (4), 1443–1458.

Dai, L., Zhou, H., Xu, X., Zuo, Z., 2019. Brain structural and functional changes in patients with major depressive disorder: a literature review. PeerJ 7, e8170.

Damaraju, E., Allen, E.A., Belger, A., Ford, J.M., McEwen, S., Mathalon, D.H., Calhoun, V.D., 2014. Dynamic functional connectivity analysis reveals transient states of dysconnectivity in schizophrenia. Neuroimage Clin 5, 298–308.

de Filippis, R., Carbone, E.A., Gaetano, R., Bruni, A., Pugliese, V., Segura-Garcia, C., De Fazio, P., 2019. Machine learning techniques in a structural and functional MRI diagnostic approach in schizophrenia: a systematic review. Neuropsychiatric Dis. Treat. 15, 1605–1627.

DeWitt, S.J., Bradley, K.A., Lin, N., Yu, C., Gabbay, V., 2018. A pilot resting-state functional connectivity study of the kynurenine pathway in adolescents with depression and healthy controls. J. Affect. Disord. 227, 752–758.

Ecker, C., Marquand, A., Mourao-Miranda, J., Johnston, P., Daly, E.M., Brammer, M.J., Murphy, D.G., 2010. Describing the brain in autism in five dimensions–magnetic resonance imaging-assisted diagnosis of autism spectrum disorder using a multiparameter classification approach. J. Neurosci. 30 (32), 10612–10623.

Fan, L., Li, H., Zhuo, J., Zhang, Y., Wang, J., Chen, L., Jiang, T., 2016. The human brainnetome atlas: a new brain atlas based on connectional architecture. Cerebr. Cortex 26 (8), 3508–3526.

Fang, X., Zhang, R., Bao, C., Zhou, M., Yan, W., Lu, S., Zhang, X., 2021. Abnormal regional homogeneity (ReHo) and fractional amplitude of low frequency fluctuations (fALFF) in first-episode drug-naive schizophrenia patients comorbid with depression. Brain Imaging Behav 15 (5), 2627–2636.

Feng, F., Wang, P., Zhao, K., Zhou, B., Yao, H., Meng, Q., Liu, Y., 2018. Radiomic features of hippocampal subregions in alzheimer's disease and amnestic mild cognitive impairment. Front. Aging Neurosci. 10, 290.

First, M.B., Gaebel, W., Maj, M., Stein, D.J., Kogan, C.S., Saunders, J.B., Reed, G.M., 2021. An organization- and category-level comparison of diagnostic requirements for mental disorders in ICD-11 and DSM-5. World Psychiatr. 20 (1), 34–51.

Geng, X., Xu, J., Liu, B., Shi, Y., 2018. Multivariate classification of major depressive disorder using the effective connectivity and functional connectivity. Front. Neurosci. 12, 38.

Gillies, R.J., Kinahan, P.E., Hricak, H., 2016. Radiomics: images are more than pictures, they are data. Radiology 278 (2), 563–577.

Gong, J., Wang, J., Luo, X., Chen, G., Huang, H., Huang, R., Wang, Y., 2020. Abnormalities of intrinsic regional brain activity in first-episode and chronic schizophrenia: a meta-analysis of resting-state functional MRI. J. Psychiatry Neurosci. 45 (1), 55–68.

Haijma, S.V., Van Haren, N., Cahn, W., Koolschijn, P.C., Hulshoff Pol, H.E., Kahn, R.S., 2013. Brain volumes in schizophrenia: a meta-analysis in over 18 000 subjects. Schizophr. Bull. 39 (5), 1129–1138.

Hong, S.J., Bernhardt, B.C., Caldairou, B., Hall, J.A., Guiot, M.C., Schrader, D., Bernasconi, A., 2017. Multimodal MRI profiling of focal cortical dysplasia type II. Neurology 88 (8), 734–742.

Hu, M.L., Zong, X.F., Mann, J.J., Zheng, J.J., Liao, Y.H., Li, Z.C., Tang, J.S., 2017. A review of the functional and anatomical default mode network in schizophrenia. Neurosci. Bull. 33 (1), 73–84.

Hu, X., Zhang, L., Bu, X., Li, H., Li, B., Tang, W., Huang, X., 2019. Localized connectivity in obsessive-compulsive disorder: an investigation combining univariate and multivariate pattern analyses. Front. Behav. Neurosci. 13, 122.

Jiang, W., Lei, Y., Wei, J., Yang, L., Wei, S., Yin, Q., Guo, W., 2019. Alterations of interhemispheric functional connectivity and degree centrality in cervical dystonia: a resting-state fMRI study. Neural Plast., 7349894
Jiang, Y., Yao, D., Zhou, J., Tan, Y., Huang, H., Wang, M., Luo, C., 2020. Characteristics of disrupted topological organization in white matter functional connectome in schizophrenia. Psychol. Med. 1–11.
Lambin, P., Rios-Velazquez, E., Leijenaar, R., Carvalho, S., van Stiphout, R.G., Granton, P., Aerts, H.J., 2012. Radiomics: extracting more information from medical images using advanced feature analysis. Eur. J. Cancer 48 (4), 441–446.
Li, J., Sun, Y., Huang, Y., Bezerianos, A., Yu, R., 2019a. Machine learning technique reveals intrinsic characteristics of schizophrenia: an alternative method. Brain Imaging Behav 13 (5), 1386–1396.
Li, M., Liu, Y., Chen, H., Hu, G., Yu, S., Ruan, X., Xie, Y., 2019b. Altered global synchronizations in patients with Parkinson's disease: a resting-state fMRI study. Front. Aging Neurosci. 11, 139.
Li, A., Zalesky, A., Yue, W., Howes, O., Yan, H., Liu, Y., Liu, B., 2020. A neuroimaging biomarker for striatal dysfunction in schizophrenia. Nat. Med. 26 (4), 558–565.
Lin, H., Cai, X., Zhang, D., Liu, J., Na, P., Li, W., 2020. Functional connectivity markers of depression in advanced Parkinson's disease. Neuroimage Clin 25, 102130.
Liu, Y., Guo, W., Zhang, Y., Lv, L., Hu, F., Wu, R., Zhao, J., 2018. Decreased resting-state interhemispheric functional connectivity correlated with neurocognitive deficits in drug-naive first-episode adolescent-onset schizophrenia. Int. J. Neuropsychopharmacol. 21 (1), 33–41.
Lu, F., Wang, M., Xu, S., Chen, H., Yuan, Z., Luo, L., Zhou, J., 2021. Decreased interhemispheric resting-state functional connectivity in male adolescents with conduct disorder. Brain Imaging Behav 15 (3), 1201–1210.
Luo, Y., He, H., Duan, M., Huang, H., Hu, Z., Wang, H., Luo, C., 2019. Dynamic functional connectivity strength within different frequency-band in schizophrenia. Front. Psychiatr. 10, 995.
Ma, X., Zheng, W., Li, C., Li, Z., Tang, J., Yuan, L., Chen, X., 2019. Decreased regional homogeneity and increased functional connectivity of default network correlated with neurocognitive deficits in subjects with genetic high-risk for schizophrenia: a resting-state fMRI study. Psychiatr. Res. 281, 112603.
Mingoia, G., Wagner, G., Langbein, K., Maitra, R., Smesny, S., Dietzek, M., Nenadic, I., 2012. Default mode network activity in schizophrenia studied at resting state using probabilistic ICA. Schizophr. Res. 138 (2-3), 143–149.
Mo, J., Liu, Z., Sun, K., Ma, Y., Hu, W., Zhang, C., Tian, J., 2019. Automated detection of hippocampal sclerosis using clinically empirical and radiomics features. Epilepsia 60 (12), 2519–2529.
Oh, K., Kim, W., Shen, G., Piao, Y., Kang, N.I., Oh, I.S., Chung, Y.C., 2019. Classification of schizophrenia and normal controls using 3D convolutional neural network and outcome visualization. Schizophr. Res. 212, 186–195.
Orban, P., Dansereau, C., Desbois, L., Mongeau-Perusse, V., Giguere, C.E., Nguyen, H., Bellec, P., 2018. Multisite generalizability of schizophrenia diagnosis classification based on functional brain connectivity. Schizophr. Res. 192, 167–171.
Plis, S.M., Amin, M.F., Chekroud, A., Hjelm, D., Damaraju, E., Lee, H.J., Calhoun, V.D., 2018. Reading the (functional) writing on the (structural) wall: multimodal fusion of brain structure and function via a deep neural network based translation approach reveals novel impairments in schizophrenia. Neuroimage 181, 734–747.
Qiu, S., Joshi, P.S., Miller, M.I., Xue, C., Zhou, X., Karjadi, C., Kolachalama, V.B., 2020. Development and validation of an interpretable deep learning framework for Alzheimer's disease classification. Brain 143 (6), 1920–1933.
Rahaman, M.A., Chen, J., Fu, Z., Lewis, N., Iraji, A., Calhoun, V.D., 2021. Multi-modal deep learning of functional and structural neuroimaging and genomic data to predict mental illness. Annu Int Conf IEEE Eng Med Biol Soc 2021, 3267–3272.
Rahaman, M.A., Damaraju, E., Turner, J.A., van Erp, T.G.M., Mathalon, D., Vaidya, J., Calhoun, V.D., 2022. Tri-clustering dynamic functional network connectivity identifies significant schizophrenia effects across multiple states in distinct subgroups of individuals. Brain Connect. 12 (1), 61–73.
Rashid, B., Calhoun, V., 2020. Towards a brain-based predictome of mental illness. Hum. Brain Mapp. 41 (12), 3468–3535.
Reed, G.M., First, M.B., Kogan, C.S., Hyman, S.E., Gureje, O., Gaebel, W., Saxena, S., 2019. Innovations and changes in the ICD-11 classification of mental, behavioural and neurodevelopmental disorders. World Psychiatr. 18 (1), 3–19.
Rosenberg, M.D., Finn, E.S., Scheinost, D., Papademetris, X., Shen, X., Constable, R.T., Chun, M.M., 2016. A neuromarker of sustained attention from whole-brain functional connectivity. Nat. Neurosci. 19 (1), 165–171.
Schneider, F.C., Royer, A., Grosselin, A., Pellet, J., Barral, F.G., Laurent, B., Lang, F., 2011. Modulation of the default mode network is task-dependant in chronic schizophrenia patients. Schizophr. Res. 125 (2-3), 110–117.
Shan, X., Liao, R., Ou, Y., Ding, Y., Liu, F., Chen, J., Guo, W., 2021. Increased homotopic connectivity in the prefrontal cortex modulated by olanzapine predicts therapeutic efficacy in patients with schizophrenia. Neural Plast. 2021, 9954547.
Shen, X., Tokoglu, F., Papademetris, X., Constable, R.T., 2013. Groupwise whole-brain parcellation from resting-state fMRI data for network node identification. Neuroimage 82, 403–415.
Shi, D., Li, Y., Zhang, H., Yao, X., Wang, S., Wang, G., Ren, K., 2021a. Machine learning of schizophrenia detection with structural and functional neuroimaging. Dis. Markers 2021, 9963824.
Shi, D., Zhang, H., Wang, G., Wang, S., Yao, X., Li, Y., Ren, K., 2022. Machine learning for detecting Parkinson's disease by resting-state functional magnetic resonance imaging: a multicenter radiomics analysis. Front. Aging Neurosci. 14, 806828.
Shi, D., Zhang, H., Wang, S., Wang, G., Ren, K., 2021b. Application of functional magnetic resonance imaging in the diagnosis of Parkinson's disease: a histogram analysis. Front. Aging Neurosci. 13, 624731.
Shu, Z.Y., Cui, S.J., Wu, X., Xu, Y., Huang, P., Pang, P.P., Zhang, M., 2021. Predicting the progression of Parkinson's disease using conventional MRI and machine learning: an application of radiomic biomarkers in whole-brain white matter. Magn. Reson. Med. 85 (3), 1611–1624.
Simpson, E.H., Kellendonk, C., Kandel, E., 2010. A possible role for the striatum in the pathogenesis of the cognitive symptoms of schizophrenia. Neuron 65 (5), 585–596.
Sun, H., Chen, Y., Huang, Q., Lui, S., Huang, X., Shi, Y., Gong, Q., 2018. Psychoradiologic utility of mr imaging for diagnosis of attention deficit hyperactivity disorder: a radiomics analysis. Radiology 287 (2), 620–630.
Sun, Y., Collinson, S.L., Suckling, J., Sim, K., 2019. Dynamic reorganization of functional connectivity reveals abnormal temporal efficiency in schizophrenia. Schizophr. Bull. 45 (3), 659–669.
Talai, A.S., Sedlacik, J., Boelmans, K., Forkert, N.D., 2021. Utility of multi-modal MRI for differentiating of Parkinson's disease and progressive supranuclear palsy using machine learning. Front. Neurol. 12, 648548.
Tang, Y., Zhou, Q., Chang, M., Chekroud, A., Gueorguieva, R., Jiang, X., Driesen, N.R., 2019. Altered functional connectivity and low-frequency signal fluctuations in early psychosis and genetic high risk. Schizophr. Res. 210, 172–179.
Tian, Z.Y., Qian, L., Fang, L., Peng, X.H., Zhu, X.H., Wu, M., Shao, J., 2020. Frequency-specific changes of resting brain activity in Parkinson's disease: a machine learning approach. Neuroscience 436, 170–183.
Tohid, H., Faizan, M., Faizan, U., 2015. Alterations of the occipital lobe in schizophrenia. Neurosciences 20 (3), 213–224.
Tzourio-Mazoyer, N., Landeau, B., Papathanassiou, D., Crivello, F., Etard, O., Delcroix, N., Joliot, M., 2002. Automated anatomical labeling of activations in SPM using a macroscopic anatomical parcellation of the MNI MRI single-subject brain. Neuroimage 15 (1), 273–289.
Umeh, A., Kumar, J., Francis, S.T., Liddle, P.F., Palaniyappan, L., 2020. Global fMRI signal at rest relates to symptom severity in schizophrenia. Schizophr. Res. 220, 281–282.
Wang, M., Hao, X., Huang, J., Wang, K., Shen, L., Xu, X., Liu, M., 2020a. Hierarchical structured sparse learning for schizophrenia identification. Neuroinformatics 18 (1), 43–57.
Wang, Y., Sun, K., Liu, Z., Chen, G., Jia, Y., Zhong, S., Tian, J., 2020b. Classification of unmedicated bipolar disorder using whole-brain functional activity and connectivity: a radiomics analysis. Cerebr. Cortex 30 (3), 1117–1128.
Weber, S., Johnsen, E., Kroken, R.A., Loberg, E.M., Kandilarova, S., Stoyanov, D., Hugdahl, K., 2020. Dynamic functional connectivity patterns in schizophrenia and the relationship with hallucinations. Front. Psychiatr. 11, 227.
Wen, D., Wang, J., Yao, G., Liu, S., Li, X., Li, J., Xu, Y., 2021. Abnormality of subcortical volume and resting functional connectivity in adolescents with early-onset and prodromal schizophrenia. J. Psychiatr. Res. 140, 282–288.
Wu, F., Zhang, Y., Yang, Y., Lu, X., Fang, Z., Huang, J., Wu, K., 2018. Structural and functional brain abnormalities in drug-naive, first-episode, and chronic patients with schizophrenia: a multimodal MRI study. Neuropsychiatric Dis. Treat. 14, 2889–2904.
Wulff, S., Nielsen, M.O., Rostrup, E., Svarer, C., Jensen, L.T., Pinborg, L., Glenthoj, B.Y., 2020. The relation between dopamine D2 receptor blockade and the brain reward system: a longitudinal study of first-episode schizophrenia patients. Psychol. Med. 50 (2), 220–228.
Xiao, Y., Yan, Z., Zhao, Y., Tao, B., Sun, H., Li, F., Lui, S., 2019. Support vector machine-based classification of first episode drug-naive schizophrenia patients and healthy controls using structural MRI. Schizophr. Res. 214, 11–17.
Xie, Y., Xi, Y., Cui, L.B., Li, C., Xu, Y., Zhang, Y., Yin, H., 2021. Altered functional connectivity of the dentate nuclei in patients with schizophrenia. Schizophr. Res. 233, 16–23.
Xue, S.W., Yu, Q., Guo, Y., Song, D., Wang, Z., 2019. Resting-state brain entropy in schizophrenia. Compr. Psychiatr. 89, 16–21.
Yan, C.G., Wang, X.D., Zuo, X.N., Zang, Y.F., 2016. DPABI: data processing & analysis for (Resting-State) brain imaging. Neuroinformatics 14 (3), 339–351.
Yan, W., Zhang, R., Zhou, M., Lu, S., Li, W., Xie, S., Zhang, N., 2020. Relationships between abnormal neural activities and cognitive impairments in patients with drug-naive first-episode schizophrenia. BMC Psychiatr. 20 (1), 283.
Yang, G.J., Murray, J.D., Glasser, M., Pearlson, G.D., Krystal, J.H., Schleifer, C., Anticevic, A., 2017. Altered global signal topography in schizophrenia. Cerebr. Cortex 27 (11), 5156–5169.
Yang, G.J., Murray, J.D., Repovs, G., Cole, M.W., Savic, A., Glasser, M.F., Anticevic, A., 2014. Altered global brain signal in schizophrenia. Proc. Natl. Acad. Sci. U. S. A. 111 (20), 7438–7443.
Yang, X., Hu, X., Tang, W., Li, B., Yang, Y., Gong, Q., Huang, X., 2019. Multivariate classification of drug-naive obsessive-compulsive disorder patients and healthy controls by applying an SVM to resting-state functional MRI data. BMC Psychiatr. 19 (1), 210.
Yin, T., Sun, R., He, Z., Chen, Y., Yin, S., Liu, X., Zeng, F., 2021. Subcortical-Cortical functional connectivity as a potential biomarker for identifying patients with functional dyspepsia. Cerebr. Cortex.
Zang, J., Huang, Y., Kong, L., Lei, B., Ke, P., Li, H., Wu, K., 2021. Effects of brain atlases and machine learning methods on the discrimination of schizophrenia patients: a multimodal MRI study. Front. Neurosci. 15, 697168.
Zeng, L.L., Wang, H., Hu, P., Yang, B., Pu, W., Shen, H., Hu, D., 2018. Multi-site diagnostic classification of schizophrenia using discriminant deep learning with functional connectivity MRI. EBioMedicine 30, 74–85.
Zhang, J., Gao, Y., He, X., Feng, S., Hu, J., Zhang, Q., Wang, L., 2021. Identifying Parkinson's disease with mild cognitive impairment by using combined MR imaging and electroencephalogram. Eur. Radiol. 31 (10), 7386–7394.
Zhang, Q., Shu, Y., Li, X., Xiong, C., Li, P., Pang, Y., Zhang, X., 2019. Resting-state functional magnetic resonance study of primary open-angle glaucoma based on voxelwise brain network degree centrality. Neurosci. Lett. 712, 134500.

Zhang, Z., Zhuo, K., Xiang, Q., Sun, Y., Suckling, J., Wang, J., Sun, Y., 2021. Dynamic functional connectivity and its anatomical substrate reveal treatment outcome in first-episode drug-naive schizophrenia. Transl. Psychiatry 11 (1), 282.

Zhao, K., Ding, Y., Han, Y., Fan, Y., Alexander-Bloch, A.F., Han, T., Liu, Y., 2020. Independent and reproducible hippocampal radiomic biomarkers for multisite Alzheimer's disease: diagnosis, longitudinal progress and biological basis. Sci. Bull. 65 (13), 1103–1113.

Zhao, X., Yao, J., Lv, Y., Zhang, X., Han, C., Chen, L., Sui, Y., 2019. Abnormalities of regional homogeneity and its correlation with clinical symptoms in Naive patients with first-episode schizophrenia. Brain Imaging Behav 13 (2), 503–513.

Zheng, J., Wei, X., Wang, J., Lin, H., Pan, H., Shi, Y., 2021. Diagnosis of schizophrenia based on deep learning using fMRI. Comput. Math. Methods Med. 2021, 8437260.

Zhao, F., Zhang, H., Rekik, I., An, Z., Shen, D., 2018a. Diagnosis of autism spectrum disorders using multi-level high-order functional networks derived from resting-state functional MRI. Front. Hum. Neurosci. 12, 184.

Zhao, C., Zhu, J., Liu, X., Pu, C., Lai, Y., Chen, L., Hong, N., 2018b. Structural and functional brain abnormalities in schizophrenia: a cross-sectional study at different stages of the disease. Prog. Neuro-Psychopharmacol. Biol. Psychiatry 83, 27–32.

Zheng, Y., Chen, X., Li, D., Liu, Y., Tan, X., Liang, Y., Shen, D., 2019. Treatment-naive first episode depression classification based on high-order brain functional network. J. Affect. Disord. 256, 33–41.

Zhou, B., An, D., Xiao, F., Niu, R., Li, W., Li, W., Lei, D., 2020a. Machine learning for detecting mesial temporal lobe epilepsy by structural and functional neuroimaging. Front. Med. 14 (5), 630–641.

Zhou, Z., Chen, X., Zhang, Y., Hu, D., Qiao, L., Yu, R., Shen, D., 2020b. A toolbox for brain network construction and classification (BrainNetClass). Hum. Brain Mapp. 41 (10), 2808–2826.